Mechanism of Flavin Mononucleotide Cofactor Binding to the *Desulfovibrio vulgaris* Flavodoxin. 2. Evidence for Cooperative Conformational Changes Involving Tryptophan 60 in the Interaction between the Phosphate- and Ring-Binding Subsites†

Tracey Arnold Murray, Mark P. Foster, and Richard P. Swenson*

Department of Biochemistry and Ohio State Biochemistry Program, The Ohio State University, Columbus, Ohio 43210

Received October 8, 2002; Revised Manuscript Received December 18, 2002

ABSTRACT: A mechanism has been proposed for the binding of flavin mononucleotide (FMN) and riboflavin to the apoflavodoxin from *Desulfovibrio vulgaris* [Murray, T. A., and Swenson, R. P. (2003) *Biochemistry 42*, 2307−2316]. In this model, the binding of the flavin isoalloxazine ring is dependent on the presence of a phosphate moiety in the phosphate-binding subsite, suggesting a cooperative interaction between that region and the ring-binding subsite. In the absence of inorganic phosphate, FMN can bind through the initial association of its 5′-phosphate group in the phosphate-binding subsite followed by insertion of the flavin ring. Because riboflavin lacks the 5′-phosphate group, it is unable to bind to this apoprotein in the absence of inorganic phosphate in solution. However, inorganic phosphate can enhance the rate of ring binding by occupying the phosphate-binding subsite. In this paper, NMR, near-UV circular dichroism (CD), and fluorescence spectroscopy provide evidence for a phosphate-induced conformational change within the isoalloxazine ring-binding subsite. Phosphate-dependent changes in the chemical shifts of 22 amide groups were observed in $^{1}H-^{15}N$ HSQC NMR spectra. The majority of these groups are proximal to the phosphate-binding subsite or the loops that constitute the isoalloxazine ring-binding site. Also, a phosphate-dependent change in the environment or position of the Trp60 side chain was apparent in the NMR data and was confirmed by associated changes in the near-UV CD and tryptophan fluorescence spectra when compared to the spectra of the W60A mutant. These data suggest that phosphate, either the 5′-phosphate of the FMN or inorganic phosphate from solution, facilitates the movement of the side chain of Trp60 out of the isoalloxazine ring-binding site and other associated conformational changes, creating a population of apoflavodoxin that is capable of binding the isoalloxazine ring. This conformational switch may explain why some apoflavodoxins cannot bind riboflavin and also supports the "aromatic gate" model proposed from the crystal structure of the *Anabaena* apoflavodoxin [Genzor, C. G., Perales-Alcon, A., Sancho, J., and Romero, A. (1996) *Nat. Struct. Biol. 3*, 329−332].

The study of flavodoxin as a model system for flavin mononucleotide (FMN)[1]-binding domains in more complex flavoproteins has resulted in a better understanding of the remarkable cooperative interactions that occur between protein and flavin and how these interactions influence the properties of the bound cofactor. These studies have been greatly facilitated by the availability of high-quality X-ray crystal structures for several holoflavodoxins, often in all three redox states of the cofactor (*1*, *2*). The cofactor-binding site in the flavodoxin and related FMN domains is primarily formed by three polypeptide loops. One loop forms an unusual binding site for the 5′-ribityl phosphate of the cofactor (the phosphate-binding subsite) through several hydrogen bonding interactions, but without ion pairing. Two other loops form the majority of the binding site for the flavin isoalloxazine ring (the ring-binding subsite). In *Desulfovibrio vulgaris* flavodoxin, this site consists of the 60's and 90's loops, which contribute all of the hydrogen bonding interactions with the ring as well as two aromatic residues that flank either face of the flavin ring (*3*−*5*). Despite this structural information, little is known about the mechanism for the binding of the cofactor to the apoflavodoxin, and many aspects remain a matter of some debate. The X-ray crystal structure of the *Anabaena* apoflavodoxin has recently provided some insight. The presence of a closed isoalloxazine ring-binding subsite and a preformed phosphate-binding subsite led the authors to propose that the 5′-phosphate moiety of the FMN initiates the binding of the cofactor to the apoflavodoxin (*6*). However, an NMR study of the flavodoxin from *Azotobacter vinelandii* suggests that the loop regions of the apoflavodoxin are very flexible and that the crystal structure may not be representative of the apoflavodoxin solution structure (*7*).

† This study was supported in part by Grant GM36490 from the National Institutes of Health.

* To whom correspondence should be addressed: Department of Biochemistry, 776 Biological Sciences Bldg., The Ohio State University, 484 W. 12th Ave., Columbus, OH 43210-1292. Telephone: (614) 292-9428. Fax: (614) 292-6773. E-mail: swenson.1@osu.edu.

[1] Abbreviations: FMN, flavin mononucleotide; CD, circular dichroism; HSQC, heteronuclear single-quantum correlation spectroscopy; DSS, 2,2-dimethyl-2-silapentane-5-sulfonic acid; NOE, nuclear Overhauser effect.

10.1021/bi026968k CCC: $25.00
Published on Web 02/04/2003

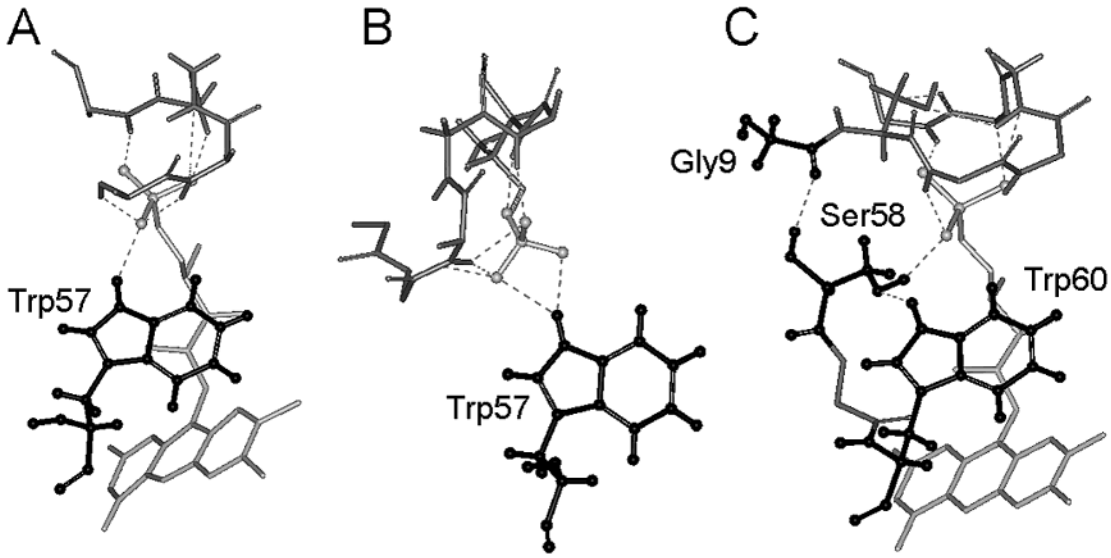

FIGURE 1: Representations of portions of the FMN binding sites from the X-ray crystal structures for the *Anabaena* holoflavodoxin (A), the *Anabaena* apoflavodoxin (B), and the *D. vulgaris* holoflavodoxin (C). In the *Anabaena* flavodoxin, the indole ring of Trp57 is hydrogen bonded directly to the 5′-phosphate group of the FMN. In the *D. vulgaris* flavodoxin, however, the indole of the equivalent tryptophan (Trp60) hydrogen bonds to the hydroxyl group of a neighboring serine (Ser58) that, in turn, is hydrogen bonded to the phosphate group.

In the preceding paper, kinetic data were used to propose a model for the binding of FMN to the flavodoxin from *D. vulgaris*, a close homologue of the *Anabaena* protein, especially in terms of the flavin-binding site (*8*). The importance of phosphate for the binding of flavin was a striking feature of that study. Time courses of FMN binding as followed by stopped-flow fluorimetry revealed biphasic fluorescence quenching when inorganic phosphate was present in the buffer solution. The rates associated with each phase were oppositely affected by increasing phosphate concentrations: the rate of the slower phase decreased and the rate of the faster phase increased. In the absence of phosphate, only one quenching phase was observed. Similarly, only one phase was noted for riboflavin binding when inorganic phosphate was present in the buffer, while binding was not detected in the absence of phosphate. As observed for the fast phase of FMN binding, the rate of riboflavin binding increased with increasing phosphate concentrations. These data led to a model in which FMN can bind to the flavodoxin in either of two modes: the phosphate-first mode (slow phase) and the ring-first mode (fast phase), based on which moiety of the cofactor initiates the binding interaction. The data strongly indicate that a bound phosphate group, either the 5′-ribityl phosphate of the cofactor or inorganic phosphate from the buffer, is required for initiation of the binding of the isoalloxazine ring to the apoprotein. When phosphate is absent, the model suggests that the apoflavodoxin is in a conformation that does not allow ring-first binding, and the FMN must initially bind via the phosphate-first mode, which then promotes ring binding. Because riboflavin lacks the 5′-ribityl phosphate group of FMN, it can only bind through the ring-first mode and only in the presence of inorganic phosphate.

Can this mechanism be reconciled with the structural basis of cofactor binding? On the basis of the crystal structures for both the *Anabaena* holo- and apoflavodoxins, an "aromatic gate" hypothesis has been proposed (*6*, *9*). This flavodoxin has an FMN binding site homologous to the *D. vulgaris* flavodoxin, including the presence of tryptophan (Trp57) and tyrosine (Tyr94) residues at positions similar to those of Trp60 and Tyr98, respectively, in the *D. vulgaris* protein (Figure 1). In the *Anabaena* holoprotein, the indole NH group of Trp57 appears to be hydrogen-bonded directly to the phosphate moiety of the FMN molecule (Figure 1A). In the apoprotein, the side chain of Trp57, the aromatic gate, moves into and occupies a portion of the flavin isoalloxazine ring-binding site in the apoprotein (Figure 1B). Thus, these differential interactions between the phosphate moiety and the indole side chain could account for the cooperative binding effects between the phosphate-binding subsite and the structure of the ring-binding subsite that are apparent in the kinetic studies for the *D. vulgaris* flavodoxin (*8*). However, the situation in this flavodoxin is somewhat different in that the side chain indole of Trp60 does not appear to hydrogen bond directly with the phosphate of the FMN, but instead hydrogen bonds with the side chain hydroxyl of Ser58, which in turn hydrogen bonds with the phosphate moiety of the FMN (Figure 1C). In this case, the binding of a phosphate group within the phosphate-binding subsite could promote the movement of the side chain of the tryptophan out of the ring-binding pocket via changes in the position of the side chain of Ser58, facilitating the binding of the isoalloxazine ring of FMN or riboflavin. In this study, nuclear magnetic resonance (NMR) spectroscopy was used to investigate the structural changes to holoflavodoxin, the riboflavin−apoflavodoxin complex, and the apoflavodoxin itself that may be induced by phosphate binding, especially in the ring-binding subsite. These data together with near-UV circular dichroism (CD) and intrinsic tryptophan fluorescence spectroscopy of wild-type and W60A apoflavodoxin provide more direct evidence for cooperative interactions between the phosphate- and ring-binding subsites that involve Trp60 that support the aromatic gate hypothesis for cofactor binding.

EXPERIMENTAL PROCEDURES

Materials. The FMN that was used was extracted from recombinant wild-type flavodoxin from *Clostridium beijer-*

inckii and purified by anion-exchange chromatography. Riboflavin was purchased from General Biochemicals, Inc. $^{15}NH_4Cl$ was purchased from Cambridge Isotope Laboratories, Inc.; [^{13}C]glucose was from Isotec, Inc., and D_2O was from Fluka Chemicals. All other chemicals were analytical reagent grade.

Protein Expression, Purification, and Apoprotein Preparation. Purified recombinant wild-type and W60A mutant holo- and apoproteins were prepared using established protocols (*8*, *10*−*12*). ^{15}N-labeled recombinant flavodoxin was purified from transformed *Escherichia coli* cultured in minimal medium with $^{15}NH_4Cl$ as the only nitrogen source. Doubly ^{13}C- and ^{15}N-labeled flavodoxin was also prepared from host *E. coli* cells grown in minimal medium with $^{15}NH_4Cl$ as the only nitrogen source and [^{13}C]glucose as the only carbon source. Final protein preparations were greater than 95% pure based on SDS−PAGE analysis.

NMR Spectroscopy. All NMR spectra were collected at protein concentrations of approximately 1 mM in the presence of 10% D_2O. Two-dimensional ^{1}H−^{15}N HSQC spectra of the holoflavodoxin and the apoflavodoxin−riboflavin complex were recorded in 100 mM sodium phosphate buffer (pH 7.0) at 300 K. The apoflavodoxin ^{1}H−^{15}N HSQC experiments were performed in 10 mM Tris-HCl buffer containing 0, 5, 10, 20, 30, 40, 50, 80, and 100 mM sodium phosphate (pH 7.0) at 300 K with the ionic strength held constant at 176 mM by the addition of NaCl. All other NMR spectra for the holoflavodoxin, the apoflavodoxin−riboflavin complex, and the apoflavodoxin were recorded in 100 mM sodium phosphate (pH 7.0) at 293 K. All concentrations and ionic strengths listed are before the addition of D_2O to a final concentration of 10% (v/v).

The ^{1}H−^{15}N HSQC spectra were collected on a Bruker DRX 800 NMR spectrometer, and all other NMR spectra were recorded using a Bruker DRX 600 NMR spectrometer. The proton chemical shifts were referenced to TMS using the relation $\delta(H_2O) = 7.83 - T/96.9$ ppm, where T is the temperature in kelvin (*13*−*15*). The ^{15}N and ^{13}C chemical shifts were referenced indirectly by using ^{1}H/X frequency ratios of 0.101 329 118 for ammonia and 0.251 449 530 for DSS (*15*−*18*). All data were processed using NMRPipe (*19*) and analyzed using NMRView (*20*). The weighted average changes in ^{1}H and ^{15}N chemical shifts ($\Delta\delta_{avg}$) were calculated using the relation $\Delta\delta_{avg} = \{[\Delta\delta_H^2 + (\Delta\delta_N/5)^2]/2\}^{1/2}$ (*21*).

NMR Parameters. The time domain sizes in points of the ^{1}H−^{15}N HSQC spectra (*22*) were 2048 for hydrogen and 128 for nitrogen, with spectral widths of 14 367.816 and 4865.0 Hz, respectively. For both the ^{1}H−^{13}C HSQC (*23*) and constant-time ^{1}H−^{13}C HSQC spectra (*24*), the time domain sizes were 1024 for hydrogen and 256 for carbon and the spectral widths were 12 500 and 12 019.231 Hz, respectively. The three-dimensional (3D) ^{1}H−^{15}N NOESY-HSQC spectrum (*25*) was acquired with time domain sizes of 1024 (HN) × 64 (N) × 300 (H) points. The spectral widths were 6410.256 (HN), 2432.65 (N), and 10 869.57 Hz (H). The NOE mixing time was 100 ms. The ^{1}H−^{15}N TOCSY-HSQC spectrum (*25*) was recorded with 1024 (HN) × 60 (N) × 200 (H) points, with spectral widths of 6410.256 (HN), 2432.646 (N), and 10 869.565 Hz (H). Isotropic mixing was achieved with a DIPSI-2rc pulse scheme (*26*) with a nominal field strength of 10 kHz and a mixing time of 43.2 ms. In the HNCACB spectrum (*27*), the time domain sizes consisted of 1024 (H) × 128 (C) × 58 (N) points, with spectral widths of 12 500.0, 9057.97, and 2587.99 Hz, respectively. The CBCA(CO)NH spectrum (*28*) was acquired with time domain sizes of 1024 (H) × 104 (C) × 64 (N) points, and the corresponding spectral widths were 12 500.0, 9057.9, and 2735.23 Hz, respectively. Last, in the HBHA(CBCACO)NH spectrum (*29*), the time domains were 512 (HN) × 128 (H) × 64 (N) points with spectral widths of 6250.0 (HN), 3987.241 (H), and 2735.23 Hz (N).

Near-UV CD Spectroscopy. All CD spectra were recorded at 25 °C using an AVIV CD spectrometer (model 62A DS) with a xenon lamp source. The concentration of apoprotein used was approximately 6 mg/mL, and the path length was 5 mm. Solutions were buffered at pH 7.0 using 38.3 mM Tris-HCl containing the desired concentration of phosphate (0 or 150 mM) and the amount of NaCl needed to keep the ionic strength constant at 300 mM. CD spectra were recorded from 250 to 320 nm at 3 s/nm. Eighty scans were averaged for wild-type apoflavodoxin in the 0 and 150 mM phosphate solutions. Eighty scans were also averaged for the W60A apoflavodoxin spectra in 0 mM phosphate solution, and 40 scans were averaged for W60A apoflavodoxin in 150 mM phosphate solution. A four-point average filtering technique was used to smooth the CD spectra.

Tryptophan Fluorescence. The intrinsic fluorescence of the two tryptophans in *D. vulgaris* flavodoxin was measured on a Jobin Yvon Horiba Fluoromax 3 spectrofluorimeter. Sample solutions were prepared by adding 10 μL of a 300−500 μM stock solution of either wild-type or W60A apoflavodoxin in 0 mM sodium phosphate solution (pH 7.0) to 2.490 mL of buffers containing 0, 10, 25, 50, 75, 100, and 150 mM sodium phosphate, 38.3 mM Tris-HCl, and the amount of NaCl necessary to keep the ionic strength constant at 300 mM. All the experiments were performed at 25 °C with a fluorescence excitation wavelength of 295 nm. The fluorescence emission was scanned from 300 to 450 nm. The fluorescence emission spectrum of Trp60 was obtained by subtraction of the spectrum of W60A from that of the wild type.

RESULTS

Holoflavodoxin Assignments. The ^{1}H and ^{15}N assignments of the holoflavodoxin from *D. vulgaris* have been established in 10 mM potassium phosphate (pH 7.0) (*30*) and in 100 mM phosphate (pH 6.5) (*31*). To aid in the assignment of the riboflavin complex and the apoflavodoxin, resonance assignments in 100 mM sodium phosphate (pH 7.0) were confirmed with data from 3D ^{1}H−^{15}N NOESY-HSQC and ^{1}H−^{15}N TOCSY-HSQC spectra (Table 1S of the Supporting Information). The majority of the cross-peaks could be superimposed among the three sets of holoflavodoxin assignments, but differences were noted in the ^{1}H and ^{15}N chemical shifts of some residues in the 60's and 90's loops in the different buffer solutions as shown in Table 1. These results suggest that the loop regions of *D. vulgaris* flavodoxin are sensitive to changes in solvent conditions.

Riboflavin−Apoflavodoxin Complex Assignments. The X-ray crystal structure of the riboflavin complex of the *D. vulgaris* flavodoxin is published (*32*), but the NMR reso-

Table 1: Changes in the Chemical Shifts of Residues in *D. vulgaris* Holoflavodoxin with Changes in Buffer Conditions

	W60	G61	D62	D63	S64	E66	L67	S96	Y98	E99	Y100	F101	C102	G103
^{15}N chemical shift (ppm)														
100 mM P_i, pH 6.5[a]	131.1	110.8	122.5	121.8	114.2	126.5	124.6	125.2	122.9	122.1	119.2	129.7	124.4	103.7
10 mM P_i, pH 7.0[b]	131.6	112.1	124.2	123.3	113.6	126.8	125.3	125.6	123.2	122.1	119.2	129.8	124.6	104.2
100 mM P_i, pH 7.0[c]	131.7	114.1	126.9	126.1	111.1	126.5	125.9	125.4	122.7	121.3	118.1	129.3	124.1	104.1
^{1}H chemical shift (ppm)														
100 mM P_i, pH 6.5[a]	8.50	8.26	8.64	8.95	7.78	7.93	8.66	9.18	7.61	8.45	8.72	8.36	9.76	7.21
10 mM P_i, pH 7.0[b]	8.57	8.40	8.75	9.05	7.77	7.73	8.73	9.24	7.66	8.38	8.46	8.41	9.73	7.30
100 mM P_i, pH 7.0[c]	8.71	8.65	8.93	9.38	7.77	7.28	8.85	9.31	7.76	8.20	8.00	8.50	9.65	7.49

[a] Chemical shifts from Stockman et al. (*31*) in 100 mM sodium phosphate buffer (pH 6.5) at 300 K. [b] Chemical shifts from Knauf et al. (*30*) in 10 mM potassium phosphate buffer (pH 7.0) at 303 K. [c] Chemical shifts measured in 100 mM sodium phosphate buffer (pH 7.0) at 300 K (this work).

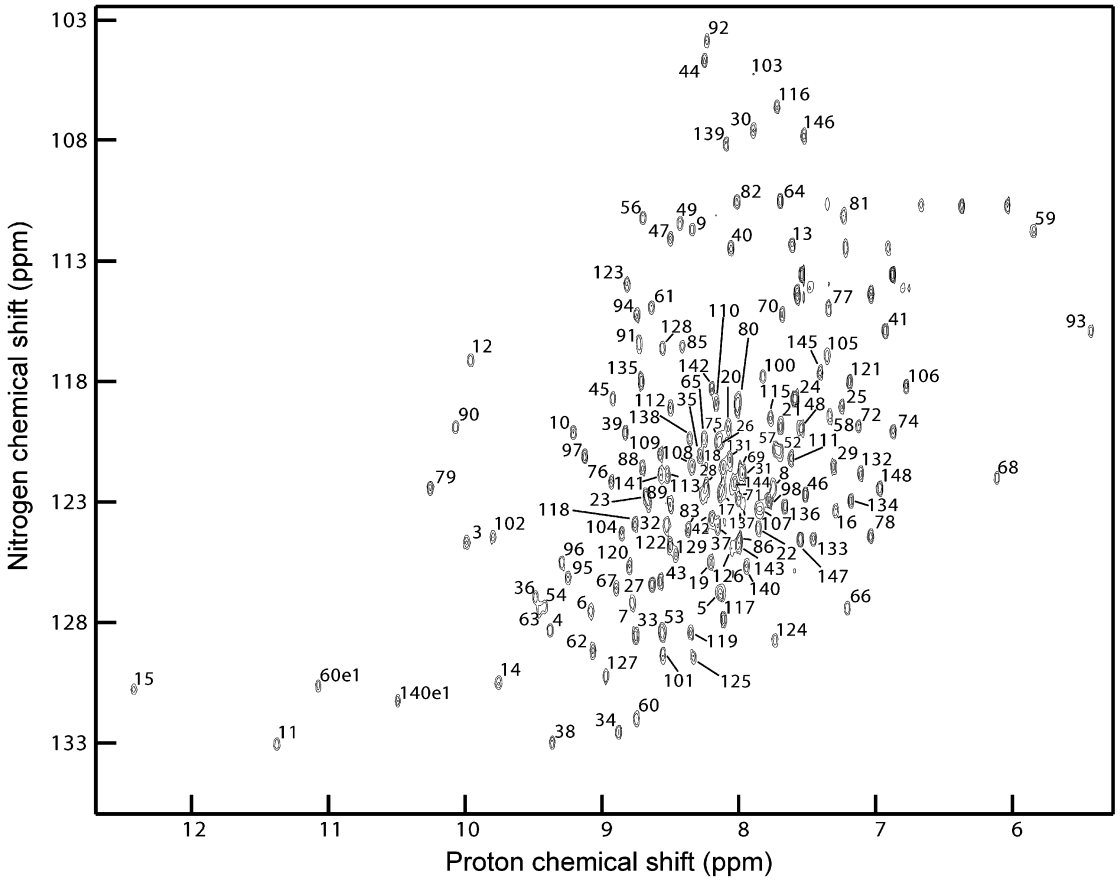

FIGURE 2: ^{1}H−^{15}N HSQC spectrum of the uniformly ^{15}N-labeled *D. vulgaris* riboflavin−apoflavodoxin complex (0.65 mM) in 90 mM sodium phosphate (pH 7.0) at 300 K in 10% D_2O at an ionic strength of 176 mM. Assigned resonances are labeled with the residue sequence number and, for the tryptophan indole cross-peaks, the atom type. The strong downfield shifts of Thr11 and Thr15 indicate the binding of an inorganic phosphate group in the FMN 5′-phosphate-binding subsite in this riboflavin complex.

nance assignments are not available. In this study, the ^{1}H and ^{15}N assignments for the riboflavin−apoflavodoxin complex were also established using ^{1}H−^{15}N NOESY-HSQC and ^{1}H−^{15}N TOCSY-HSQC data (Figure 2, and Table 2S of the Supporting Information). The weighted average amide ^{1}H and ^{15}N chemical shift changes ($\Delta\delta_{avg}$) between the holoflavodoxin (FMN) and the riboflavin complexes were determined using the equation of Garret et al. (*21*). The average (0.075) and standard deviation (0.058) of $\Delta\delta_{avg}$ of all of the amide resonances were calculated, and changes considered to be significant were those greater than one standard deviation above the average (0.132). Although 82% of the backbone amide cross-peaks superimposed when the spectrum of the riboflavin complex was compared to that of the holoflavodoxin, 24 peaks shifted with $\Delta\delta_{avg}$ values greater than or equal to 0.132 (Figure 3). All of the affected amide resonances map to the flavin-binding site or reflect propagation up the helices following the 60's and 90's loops. A repositioning of the isoalloxazine ring is apparent in the crystal structure (*32*), and the residues with changes in their chemical shifts in the NMR data confirm a different environment for this area of the solution structure. The teen's loop residues also had significant chemical shift differences when compared to those of the holoflavodoxin, with the largest changes occurring in residues Thr15 (0.42) and Thr12 (0.38). The large downfield shifts for Thr11 and Thr15 (Figure 2, and Table 2S of the Supporting Information) strongly suggest that a phosphate is bound in this position in the riboflavin complex as was observed in the X-ray crystal structure. The HSQC spectra of the riboflavin

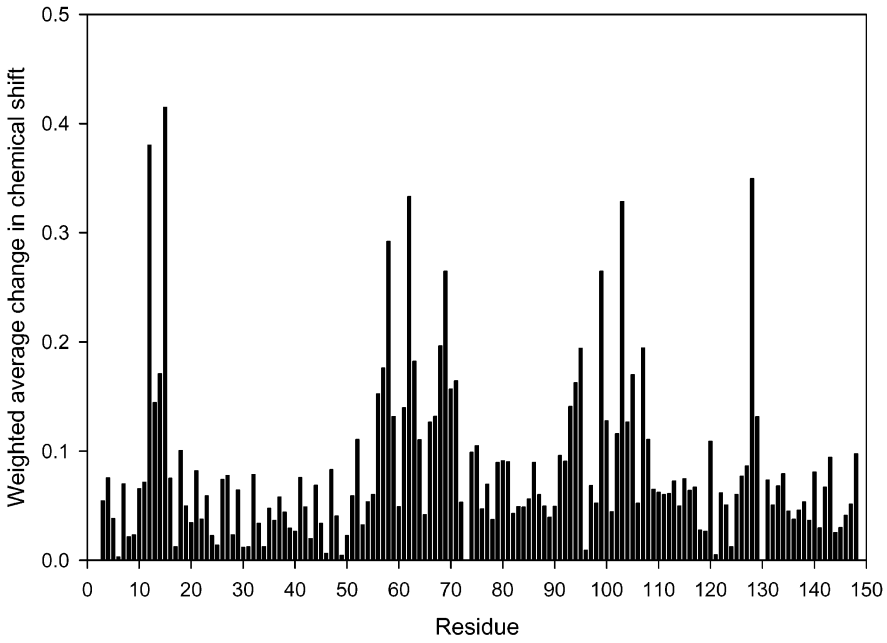

FIGURE 3: Weighted average ^{1}H and ^{15}N chemical shift changes ($\Delta\delta_{avg}$), as determined using the equation of Garrett et al. (*21*), between holoflavodoxin (FMN) and the apoflavodoxin−riboflavin complex for each residue in the complex. Changes greater than 0.132, which are considered to be statistically significant, are primarily localized to the three loops that make up the FMN-binding site.

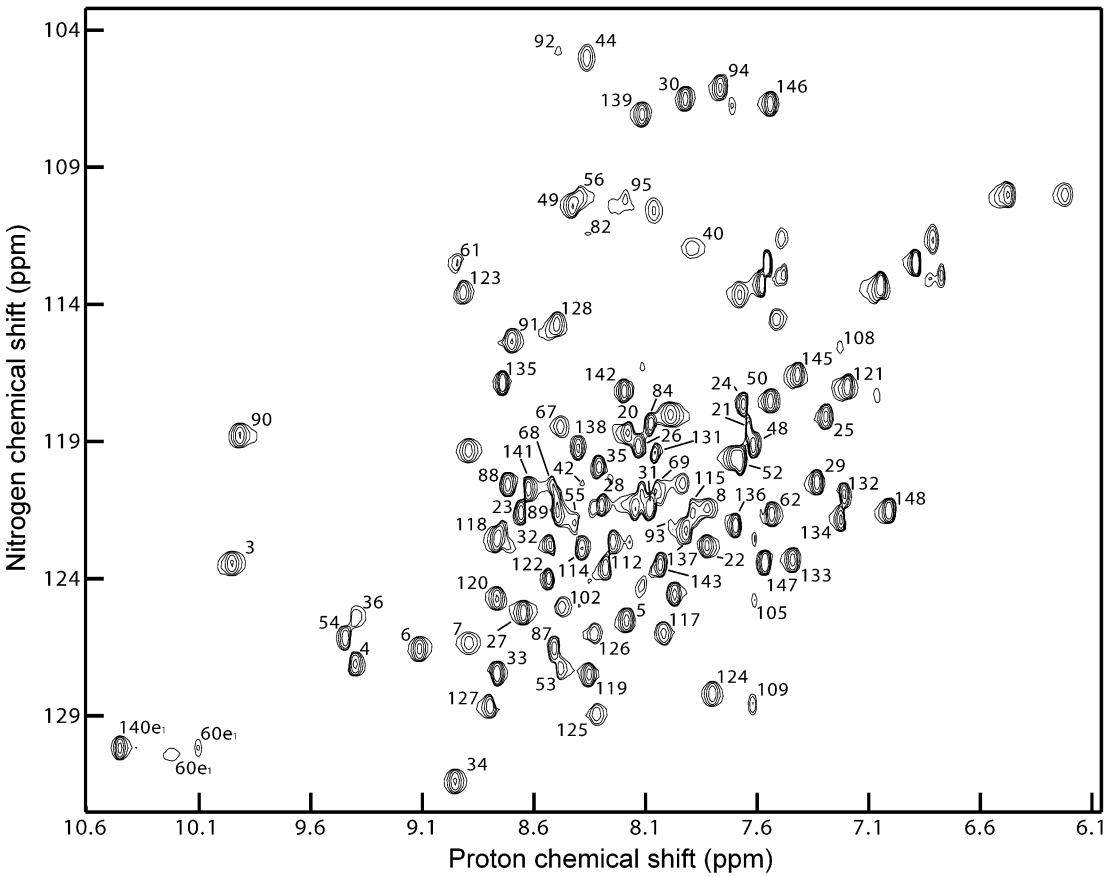

FIGURE 4: ^{1}H−^{15}N HSQC spectrum of uniformly ^{15}N-labeled *D. vulgaris* apoflavodoxin (1 mM) in 72 mM sodium phosphate and 10 mM Tris-HCl (pH 7.0) at 300 K in 10% D_2O at an ionic strength of 176 mM. Assigned resonances are labeled with the residue number and, for the tryptophan indole cross-peaks, the atom type.

complex in the presence of 5 and 50 mM sodium phosphate (pH 7.0) were also collected. These spectra were identical (data not shown), which suggests that the riboflavin complex is not affected by the concentration of free inorganic phosphate.

Apoflavodoxin Assignments. The purpose of this series of experiments was to assess any changes and alterations in the environment of specific residues in the apoflavodoxin in response to different concentrations of inorganic phosphate. The ^{1}H−^{15}N HSQC spectrum of the apoflavodoxin

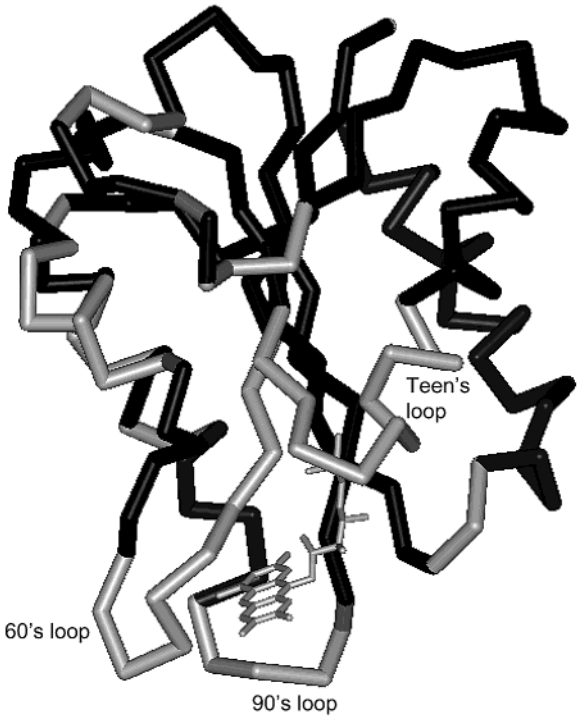

FIGURE 5: Location of the assigned amide groups of *D. vulgaris* apoflavodoxin as determined using the triple-resonance NMR spectral data. All assigned residues are represented in black on the backbone trace based on the *D. vulgaris* holoflavodoxin crystal structure, while the unassigned residues are shaded in gray. Sixty-nine percent of the residues in the apoflavodoxin are assigned.

Table 2: Residues in the *D. vulgaris* Apoflavodoxin that Display Significant Changes in the Chemical Shift Values for Their $^1H-^{15}N$ HSQC Cross-Correlation Peaks with Increasing Concentrations of Inorganic Phosphate

residue	$\Delta\delta_{avg}$ (ppm)[a]	K_d (mM)
Val7	0.10	32 ± 10
Glu20	0.10	13 ± 2
Asp34	0.06	18 ± 3
Arg36	0.11	71 ± 5
Ser40	0.11	91 ± 7
Leu55	0.11	39 ± 3
Gly56	0.10	38 ± 17
Leu67	0.08	22 ± 4
Gln68	0.09	40 ± 10
Gln84	0.07	49 ± 3
Gly85	0.10	46 ± 10
Lys87	0.07	101 ± 6
Phe91	0.07	49 ± 3
Gly94	0.08	57 ± 12
Ala117	0.08	39 ± 3
Arg125	0.07	49 ± 3
Ile126	0.07	90 ± 4
Gly128	0.10	46 ± 10
$Trp60_{indole}$[b]	0.13	101 ± 6
UA[c]	0.21	75 ± 17
UA[c]	0.13	101 ± 6
SC[d]	0.13	65 ± 23
SC[d]	0.11	25 ± 5
SC[d]/UA[c]	0.11	47 ± 15

[a] Weighted averages (including both ^1H and ^{15}N chemical shift values) were determined by the equation of Garrett et al. (*21*). Error values for $\Delta\delta_{avg}$ are ± 0.02. [b] Indole NH group of Trp60. [c] Unassigned backbone amide. [d] Unassigned side chain amides.

in 100 mM sodium phosphate (pH 7.0) is shown in Figure 4. Unfortunately, the NMR signals for the residues in the three loops surrounding the flavin were not observed in the apoflavodoxin spectrum (Figure 5) (*7*). Thus, it appears these loops are conformationally disordered on the millisecond to microsecond time scale. Also, the spectral dispersion was reduced in the spectrum of the apoprotein, resulting in significant overlap; this made intractable the assignment of some resonances, even with triple-resonance spectra. Nevertheless, the assignments for a significant portion of the apoprotein could be obtained (Figure 5, and Table 3S of the Supporting Information), yielding a great deal of information.

Phosphate Competition in Apoflavodoxin HSQCs. The $^1H-^{15}N$ HSQC spectrum of the apoflavodoxin was established in different concentrations of phosphate buffer, but at a constant ionic strength of 176 mM (before the addition of D_2O and as adjusted with the addition of NaCl). Because of declining probe performance at higher ionic strengths, experiments were performed up to a maximum phosphate concentration of 100 mM. As can be seen in Figure 6, some of the resonances did shift as the concentration of inorganic phosphate was increased; the majority, however, were unaffected by the phosphate concentration. The weighted average chemical shift change ($\Delta\delta_{avg}$) between 0 and 100 mM phosphate was calculated (*21*) for all of the cross-peaks. The average (0.036) and standard deviation (0.023) of the $\Delta\delta_{avg}$ values were measured, and significant changes were again considered to be those greater than one standard deviation above the mean (0.060). Twenty-two resonances met this criterion: 16 assigned backbone amides, two unassigned backbone amides, one assigned side chain indole NH, and three unassigned side chain amides (Table 2). All of the assigned residues with significant chemical shift changes are located near the FMN-binding site, either before or after the loops themselves, or in regions near the loops (Figure 7).

In each case, a hyperbolic curve was approximated when the $\Delta\delta_{avg}$ was plotted against the phosphate concentration, yielding an apparent dissociation constant for inorganic phosphate and apoflavodoxin (Figure 8) (*33*). A list of the residues with significant chemical shift changes (and their apparent dissociation constants) is given in Table 2. The global fit of all of the data to a single-site binding isotherm generated an apparent K_d value of 51 ± 4 mM. This value is quite similar to the apparent K_d value of 45 ± 9 mM for the apoprotein−phosphate complex observed in the kinetic studies (*8*).[2]

The resonances associated with the protons on the indole nitrogens of the tryptophan residues require further comment. When no phosphate was present in the buffer solution, there were only two signals in the "indole" region of the HSQC spectrum, corresponding to the two tryptophans in *D. vulgaris* flavodoxin (Trp60 and Trp140). However, as the phosphate concentration was increased, the signal from one of the tryptophan indole groups split into two components, one centered at the original chemical shift, the volume of

[2] Equilibrium dialysis with radiolabeled phosphate was applied in an attempt to provide more direct evidence for the binding of inorganic phosphate and to confirm this K_d value. However, the binding of radiolabeled phosphate could not be reliably detected above the high background of unbound radioactivity. In fact, the detection limit for this method under our conditions was calculated to be ≤ 30 mM, which is lower than the apparent K_d value for the apoflavodoxin−phosphate complex obtained from the NMR and kinetic data.

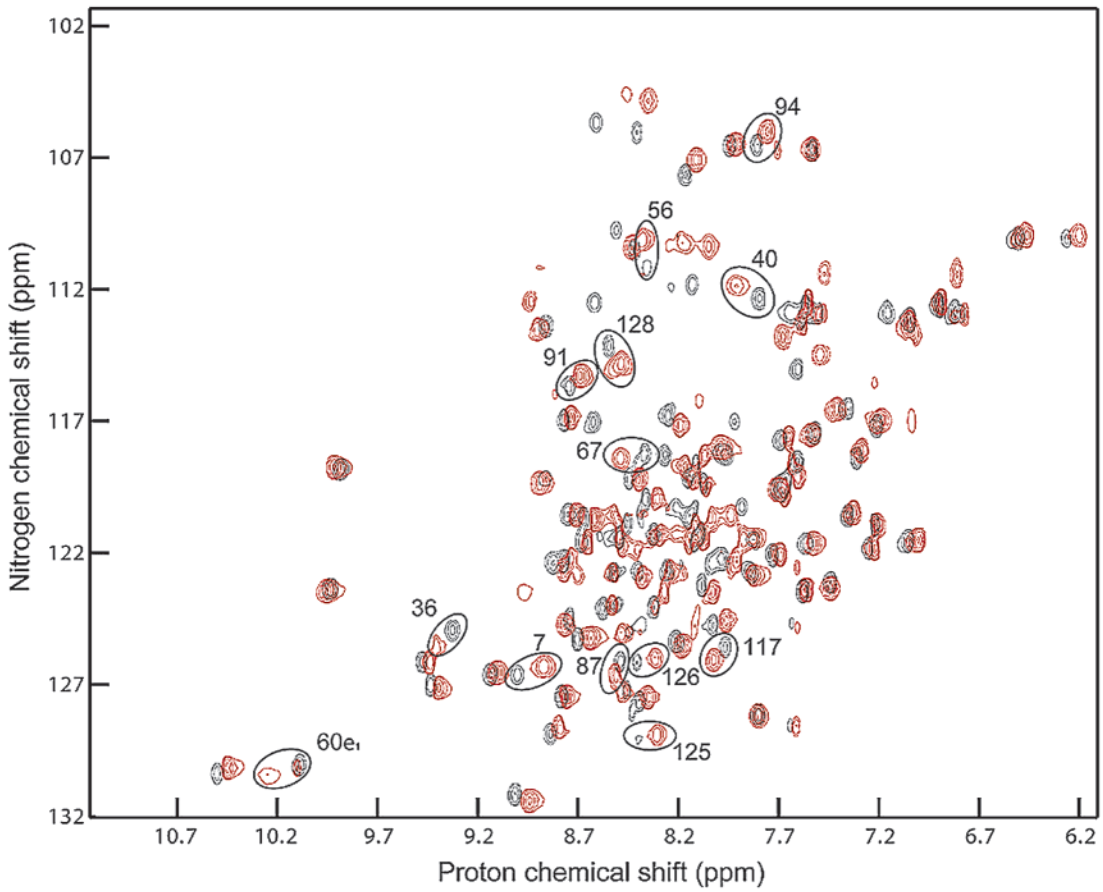

FIGURE 6: Overlaid $^{1}H-^{15}N$ HSQC spectra of uniformly ^{15}N-labeled *D. vulgaris* apoflavodoxin (1 mM) in 0 mM phosphate solution (pH 7.0) (black) and in 100 mM sodium phosphate (pH 7.0) (red). The phosphate solutions are as described in Experimental Procedures. Several representative resonances that display a significant change in their weighted average chemical shift value ($\Delta\delta_{avg}$) with increasing concentrations of inorganic phosphate are circled and labeled with the residue sequence number for clarity.

which decreased with increasing phosphate and one which emerged from the first and shifted downfield, the volume of which increased with increasing phosphate (Figure 9). On the basis of the unambiguous assignment of the backbone amide of Trp140 using three-dimensional NMR spectra, the peak less affected by the concentration of phosphate could be assigned to the indole of Trp140 using NOE connectivities to the backbone resonance. Therefore, the other two peaks were assigned to the side chain of Trp60. Thus, the reported change in chemical shift measured for the indole of Trp60 is the change in the position of the secondary peak relative to the primary peak. This change in chemical shift follows an apparent phosphate-binding isotherm, generating a value for the apparent dissociation constant that is similar to that observed from the kinetic data (Table 2).

Near-UV Circular Dichroism and Fluorescence Spectroscopy. Because of the change seen in the NMR data for Trp60, near-UV CD and tryptophan fluorescence spectroscopy were used to investigate this residue further. The near-UV CD spectrum is dominated by the absorbance of the two tryptophan residues present in *D. vulgaris* apoflavodoxin (Trp60 and Trp140). There were no differences observed in the spectra of W60A apoflavodoxin in 0 and 150 mM phosphate solutions (Figure 10B). However, differences in the near-UV CD spectrum of wild-type apoflavodoxin were noted when the concentration of phosphate was increased (with the ionic strength held constant using NaCl) (Figure 10A). There was a decrease in the molar ellipticity of the apoflavodoxin in the 150 mM phosphate solution, especially in the 250−270 and 290−300 nm regions (Figure 10C). Because there were no differences observed for W60A apoflavodoxin, the differences observed in the wild-type spectrum are very likely due to changes in the environment of Trp60 only. Decreased intensity in CD spectra is often associated with increased mobility of the residue(s) responsible for the absorbance; therefore, this decrease could be due to increased mobility of the tryptophan residue (*34*). Similarly, on the basis of the comparison of the fluorescence emission spectra of the wild-type and W60A apoflavodoxins, the fluorescence due to Trp60 increased with increasing concentrations of phosphate in the buffer (Figure 11). This, too, may be due to an increase in mobility or solvent accessibility of the residue. Thus, the CD, fluorescence, and NMR data were all indicative of a change in the environment of Trp60 as the concentration of phosphate increased.

DISCUSSION

On the basis of the kinetic studies of the flavodoxin from *D. vulgaris*, a minimal mechanistic model was proposed for the binding of FMN and riboflavin to this apoprotein (*8*). Two different binding modes were apparent in that study, which were termed the phosphate-first and ring-first binding modes. In the presence of phosphate, FMN binds by either mode but at differing rates, resulting in two fluorescence-quenching phases. However, a single kinetic phase was associated with the binding of riboflavin, which can only

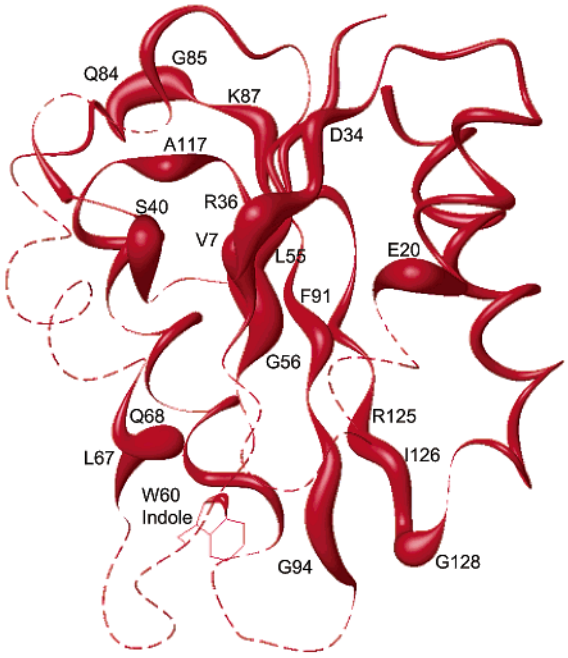

FIGURE 7: Representation of the changes in the weighted average chemical shift values ($\Delta\delta_{avg}$) as a function of the concentration of phosphate for the *D. vulgaris* apoflavodoxin. The diameter of the tube representing the peptide backbone is proportional to the value for $\Delta\delta_{avg}$; i.e., the larger the diameter, the larger the $\Delta\delta_{avg}$ value. Those residues with significant $\Delta\delta_{avg}$ values are labeled. The dashed lines represent regions of the apoprotein for which the residues could not be assigned. This figure was prepared using the program MOLMOL (*35*) and the coordinates for the *D. vulgaris* holoprotein.

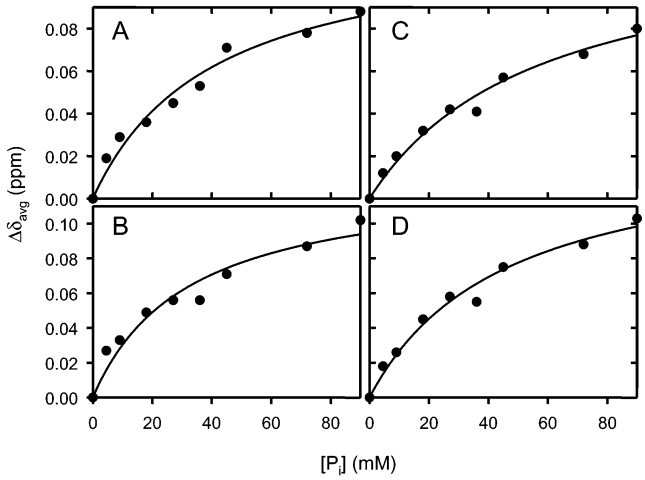

FIGURE 8: Examples of the effect of phosphate on the weighted average chemical shift values ($\Delta\delta_{avg}$) of select residues in *D. vulgaris* apoflavodoxin plotted against the phosphate concentration. The solid lines represent nonlinear regression fits of the data to a single-site binding isotherm: (A) $K_d = 40 \pm 10$ mM for Gln68, (B) $K_d = 32 \pm 10$ mM for Val7, (C) $K_d = 57 \pm 12$ mM for Gly94, and (D) $K_d = 46 \pm 10$ mM for Gly128.

bind via the ring-first mode. In the absence of inorganic phosphate in solution, the binding of FMN becomes monophasic while riboflavin does not bind appreciably. These results suggest that the ring-binding mode is dependent on the presence of inorganic phosphate and that a cooperative interaction exists between the phosphate- and ring-binding subsites.

To further investigate this hypothesis, more direct biophysical evidence for phosphate binding and cooperative conformational changes was sought. Changes in the backbone amide chemical shifts of the flavodoxin verified that inorganic phosphate is able to bind to the apoprotein with an apparent K_d value similar to that observed in the kinetic studies (*8*). The $^1H-^{15}N$ HSQC NMR data also provided information about the location of the inorganic phosphate-binding site and the regions affected by its binding. This information, together with the near-UV CD and fluorescence spectroscopic data, supports a cooperative interaction between the phosphate- and ring-binding subsites. Further insights can be obtained from these data as follows.

On the basis of the X-ray diffraction data of the apoprotein, it was expected that the binding of inorganic phosphate would perturb several amide resonances in the teen's (phosphate-binding) loop, especially the amide peaks of residues Thr11 and Thr15. Unfortunately, these resonances and others in this loop were not observed in the apoflavodoxin HSQC spectra, most likely because of flexibility (Figure 5). Phosphate binding could be expected to "stiffen" this loop, allowing for the identification of new resonance peaks that could be assigned to teen's loop residues at increased concentrations of phosphate. However, this was not observed. Given the weak binding of inorganic phosphate (with an apparent K_d of ~45 mM), the k_{off} can be expected to be too fast on the NMR time scale for these cross-peaks to be observed. However, chemical shift changes were noted in the backbone amides of Val7 and Glu20, which flank either side of the teen's loop (Figures 5 and 7). This gave a good indication that the loop between these residues was also experiencing environmental changes associated with phosphate binding and that inorganic phosphate was binding in the 5′-ribityl phosphate group subsite of the FMN binding site.

Phosphate-dependent changes were also evident in the 60's and 90's loops, which constitute much of the isoalloxazine ring-binding site. Again, because of their flexibility, most of the amide resonances in these loops were not observed. However, significant chemical shift changes were observed in residues that flank each loop, including Leu55, Gly56, Leu67, Gln68, Phe91, and Gly94 (Figures 5 and 7). Phosphate-dependent changes in the amide resonances of several other neighboring residues provided additional support for modifications in the structure of the loop regions (Figure 7). Alterations in the resonances of Asp34 and Arg36 may reflect structural changes in the teen's loop. Nearby, Ser40 also displayed a significant chemical shift change, which could have been due to the rearrangement of Asp34 and Arg36 because of their interaction with teen's loop residues. This change in Ser40 could also have been due to rearrangement of the 60's loop that was translated up the helix following the 60's loop to residues near Ser40. The same was true for Gln84, Gly85, and Lys87; the changes in the environment of these residues could have been due to propagation up this helix from the 90's loop. Ala117 is in close contact with these residues and also with Arg36 and Ser40 and thus also experiences environmental differences. Finally, Arg125, Ile126, and Gly128 are all part of a loop that is in hydrogen bonding contact with the 90's loop. Rearrangement of the 90's loop could cause the chemical shift changes observed in these residues. Thus, phosphate-dependent changes in these peaks seem to corroborate the changes in environment experienced by the 60's and 90's

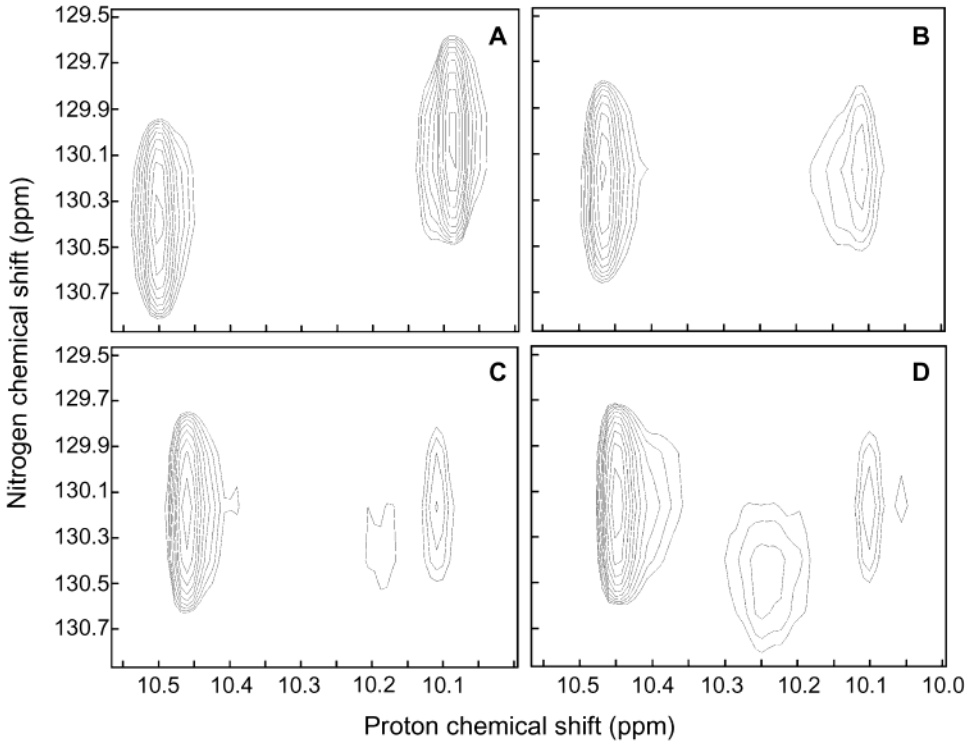

FIGURE 9: Tryptophan indole region of the $^{1}H-^{15}N$ HSQC spectra of uniformly ^{15}N-labeled *D. vulgaris* apoflavodoxin (1 mM) in 0 mM phosphate (A), 10 mM phosphate (B), 50 mM phosphate (C), and 100 mM phosphate (D) solutions at pH 7.0 and 300 K. All phosphate solutions were controlled for constant ionic strength as described in Experimental Procedures. Note that the signal from one of the tryptophan indole groups splits into two cross-peaks as the phosphate concentration increases.

loops and support the hypothesis that these loops are responding to phosphate binding to the 5′-phosphate-binding subsite of FMN.

The strongest indicator of phosphate-induced changes in the structure of the 60's loop was provided by chemical shift changes in the side chain indole of Trp60, which by analogy to the *Anabaena* flavodoxin may be part of the so-called aromatic gate for cofactor binding in this protein (*6*). Although three peaks are observed in the indole region of the HSQC spectra of the apoflavodoxin in the presence of phosphate, there are only two tryptophan residues in *D. vulgaris* flavodoxin (Figure 9). The peak less affected by phosphate was assigned to Trp140, indicating the other two peaks result from the splitting of the resonance from the side chain of Trp60. This splitting strongly suggests that, in the presence of phosphate, the side chain is sampling two distinct environments. Furthermore, as the concentration of phosphate was increased, the chemical shift of the population-weighted average shifted further from the first environment, resulting in a decrease in the volume of the original resonance peak and a corresponding increase in volume for the additional peak representing the second environment. Because the only variable in these experiments was the concentration of inorganic phosphate, two cross-peaks of the indole of Trp60, and especially the appearance of one emerging from the other, provided a strong indication of the phosphate-dependent movement of this side chain.

Two other methods were used to independently confirm this apparent phosphate-dependent conformational change for Trp60: near-UV CD and tryptophan fluorescence spectroscopy. In both cases, comparisons were made between the wild type and the W60A mutant to show that the changes in the spectra were due to Trp60. There was a decrease in the molar ellipticity of the near-UV CD spectrum for wild-type apoflavodoxin in 150 mM phosphate solution when compared to the spectrum of the wild type where no inorganic phosphate was present (Figure 10A); however, there were no differences in the spectra of W60A apoflavodoxin in solutions containing 0 or 150 mM phosphate (Figure 10B). This finding suggested that the differences in the wild-type spectrum were due to changes in the environment of Trp60. A decrease in ellipticity, as observed for the wild-type spectrum in the 150 mM phosphate solution, is suggestive of increased mobility for Trp60. Also, the fluorescence of Trp60 increases as the concentration of phosphate is increased (Figure 11). An increase in the intrinsic fluorescence is expected if Trp60 moves away from the ring-binding site and Tyr98 as phosphate binds to the apoflavodoxin.

Thus, all of the NMR, CD, and fluorescence data taken together strongly support our binding model (*8*). According to this model, Trp60 and the adjacent loop regions become more mobile when phosphate binds to the phosphate-binding subsite of the apoflavodoxin, facilitating the opening of the aromatic gate and allowing for the efficient binding of the isoalloxazine ring of the flavin cofactor. On the basis of the difference in ^{1}H chemical shift of the two populations of Trp60 indole, an upper limit on the rate of the movement of this side chain between the two states can be estimated to be 130 s^{-1}. The experimental rates for the binding of riboflavin at saturating phosphate concentrations are on the same order of magnitude or slower than this Trp60 side chain transition (*8*). Thus, these observations are consistent with the aromatic gate hypothesis and the necessary movement of the flavin binding loops and the Trp60 side chain out of the ring-binding subsite for the binding of the flavin isoalloxazine ring.

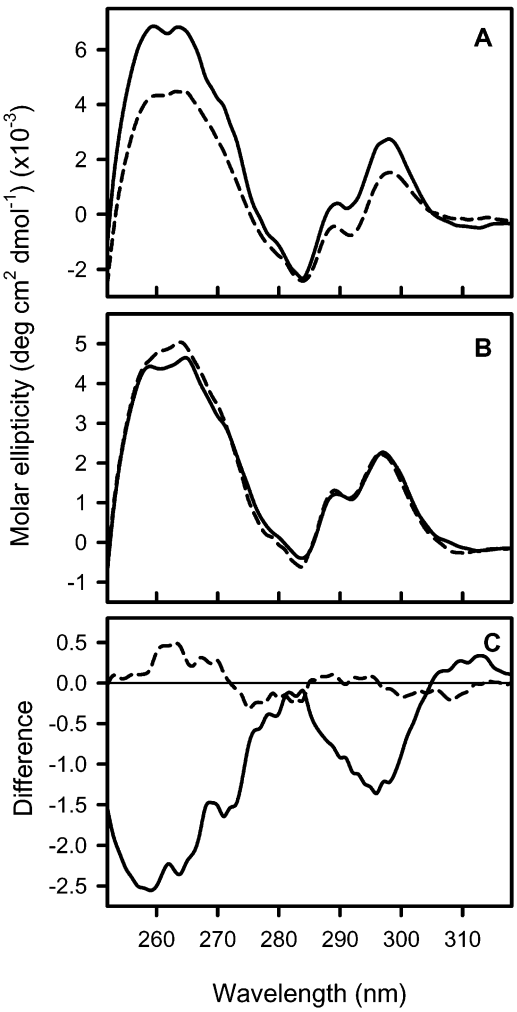

FIGURE 10: Near-UV CD spectra of wild-type (A) and W60A (B) *D. vulgaris* flavodoxins in a 0 mM phosphate solution (—) and in a 150 mM phosphate solution (– – –). The spectra were obtained using 0.5 mM protein solutions at pH 7.0, 25 °C, and an ionic strength of 300 mM in buffers described in Experimental Procedures. The difference spectra for wild-type (—) and W60A (– – –) proteins are shown in panel C. Note the differences in the wild-type spectra as a function of inorganic phosphate concentration that are not observed in the W60A mutant flavodoxin spectra.

It is difficult to establish the exact mechanism by which the opening of the aromatic gate occurs. However, it is possible that phosphate binding may cooperatively influence the structure of the flavin ring-binding subsite through the hydrogen bonding network between the side chain indole of Trp60, the side chain hydroxyl of Ser58, the backbone carbonyl of Gly9, and the phosphate ion itself. When phosphate binds to the phosphate-binding subsite, it stiffens the position of the teen's loop through its extensive hydrogen bonding network with these residues. Because Ser58 is hydrogen bonded to both the backbone of Gly9 and the phosphate ion, its position could also be stiffened by the presence of the phosphate. These interactions would help either to pull the Trp60 side chain out of the ring-binding subsite or perhaps to serve as a "latch" to hold the indole gate open, enabling the binding of the isoalloxazine ring.

Conclusions. The presence of the aromatic gate seen in the structure of the *Anabaena* apoflavodoxin gives some insight into the binding site of FMN without the cofactor present and allows mechanisms for cofactor binding to be

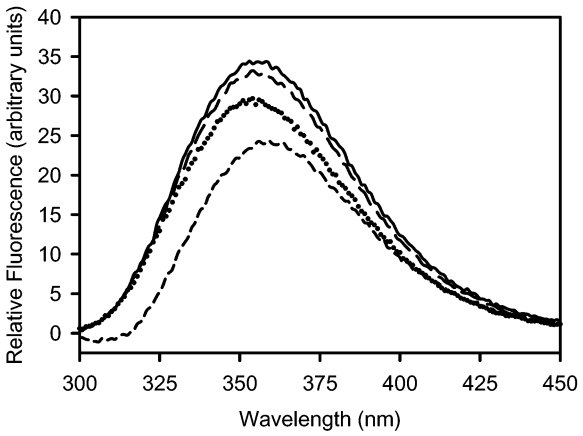

FIGURE 11: Change in the fluorescence emission spectrum of Trp60 with increasing concentrations of inorganic phosphate. The spectral changes attributed to Trp60 itself were obtained by subtracting the spectrum for the W60A mutant from that of the wild-type apoflavodoxin. All spectra were collected with an excitation wavelength of 295 nm at 25 °C, pH 7.0, and an ionic strength of 300 mM in buffer solutions containing final phosphate concentrations of 0 (- - -), 10 (•••), 50 (– – –), and 150 mM (—) as described in Experimental Procedures.

hypothesized (*6*). The kinetics research in our previous paper showed that the binding of FMN to the flavodoxin from *D. vulgaris* was biphasic and that the ring-first binding phase could only occur in the presence of inorganic phosphate (*8*). The most likely scenario was that the phosphate was binding to the phosphate-binding subsite of the FMN-binding site and this phosphate was able to "communicate" with the ring-binding portion of the FMN-binding site. The data in this paper confirm this result and show that the aromatic gate proposed in the *Anabaena* flavodoxin is most likely also present in the *D. vulgaris* apoflavodoxin. On the basis of the data, the phosphate is able to stiffen the binding loops of the flavodoxin and hold Trp60 out of the ring-binding site, creating a population of apoflavodoxin that is capable of binding the isoalloxazine ring first.

ACKNOWLEDGMENT

We acknowledge Dr. Charles E. Cottrell of the Campus Chemical Instrument Center (The Ohio State University) for his assistance in obtaining the NMR data.

SUPPORTING INFORMATION AVAILABLE

Chemical shifts of assigned ^{1}H and ^{15}N resonances of the *D. vulgaris* holoflavodoxin and the *D. vulgaris* riboflavin–apoflavodoxin complex in 100 mM sodium phosphate buffer (pH 7.0) at 293 K and the *D. vulgaris* apoflavodoxin in 100 mM sodium phosphate buffer (pH 7.0) at 300 K. This material is available free of charge via the Internet at http://pubs.acs.org.

REFERENCES

1. Mayhew, S. G., and Tollin, G. (1992) in *Chemistry and Biochemistry of Flavoenzymes* (Muller, F., Ed.) pp 389–426, CRC Press, Boca Raton, FL.
2. Ludwig, M. L., and Luschinsky, C. L. (1992) in *Chemistry and Biochemistry of Flavoenzymes* (Muller, F., Ed.) pp 427–466, CRC Press, Boca Raton, FL.
3. Watenpaugh, K. D., Sieker, L. C., Jensen, L. H., Legall, J., and Dubourdieu, M. (1972) Structure of the oxidized form of a flavodoxin at 2.5-Angstrom resolution: resolution of the phase

ambiguity by anomalous scattering, *Proc. Natl. Acad. Sci. U.S.A. 69*, 3185−3188.
4. Watenpaugh, K. D., Sieker, L. C., and Jensen, L. H. (1973) The binding of riboflavin-5′-phosphate in a flavoprotein: flavodoxin at 2.0-Angstrom resolution, *Proc. Natl. Acad. Sci. U.S.A. 70*, 3857−3860.
5. Watt, W., Tulinsky, A., Swenson, R. P., and Watenpaugh, K. D. (1991) Comparison of the crystal structures of a flavodoxin in its three oxidation states at cryogenic temperatures, *J. Mol. Biol. 218*, 195−208.
6. Genzor, C. G., Perales-Alcon, A., Sancho, J., and Romero, A. (1996) Closure of a tyrosine/tryptophan aromatic gate leads to a compact fold in apoflavodoxin, *Nat. Struct. Biol. 3*, 329−332.
7. Steensma, E., and vanMierlo, C. P. M. (1998) Structural Characterisation of Apoflavodoxin shows that the Location of the Stable Nucleus Differs Among Proteins with a Flavodoxin-like Topology, *J. Mol. Biol. 282*, 653−666.
8. Murray, T. A., and Swenson, R. P. (2003) Mechanism of Flavin Mononucleotide Cofactor Binding to the *Desulfovibrio vulgaris* Flavodoxin. 1. Kinetic Evidence for Cooperative Effects Associated with the Binding of Inorganic Phosphate and the 5′-Phosphate Moiety of the Cofactor, *Biochemistry 42*, 2307.
9. Rao, S. T., Shaffie, F., Yu, C., Satyshur, K. A., Stockman, B. J., Markley, J. L., and Sundarlingam, M. (1992) Structure of the oxidized long-chain flavodoxin from *Anabaena* 7120 at 2 Å resolution, *Protein Sci. 1*, 1413−1427.
10. Swenson, R. P., and Krey, G. D. (1994) Site-directed mutagenesis of tyrosine-98 in the flavodoxin from *Desulfovibrio vulgaris* (Hildenborough): regulation of oxidation−reduction properties of the bound FMN cofactor by aromatic, solvent, and electrostatic interactions, *Biochemistry 33*, 8505−8514.
11. Wassink, J. H., and Mayhew, S. G. (1975) Fluorescence titration with apoflavodoxin: a sensitive assay for riboflavin 5′-phosphate and flavin adenine dinucleotide in mixtures, *Anal. Biochem. 68*, 609−616.
12. Zhou, Z., and Swenson, R. P. (1996) Evaluation of the electrostatic effect of the 5′-phosphate of the flavin mononucleotide cofactor on the oxidation−reduction potentials of the flavodoxin from *Desulfovibrio vulgaris* (Hildenborough), *Biochemistry 35*, 12443−12454.
13. Hartel, A. J., Lankhorst, P. P., and Altona, C. (1982) Thermodynamics of stacking and of self-association of the dinucleoside monophosphate m2(6)A-U from proton NMR chemical shifts: differential concentration temperature profile method, *Eur. J. Biochem. 129*, 343−357.
14. Orbons, L. P. M., van der Marel, G. A., van Boom, J. H., and Altona, C. (1987) An NMR study of polymorphous behaviour of the mismatched DNA octamer d(m5C-G-m5C-G-A-G-m5C-G) in solution. The B-duplex and hairpin forms, *Eur. J. Biochem. 170*, 225−239.
15. Cavanagh, J., Fairbrother, W. J., Palmer, A. G., and Skelton, N. J. (1996) *Protein NMR Spectroscopy: Principles and Practice*, Academic Press, San Diego.
16. Live, D. H., Davis, D. G., Agosta, W. C., and Cowburn, D. (1984) Long-range hydrogen bond mediated effects in peptides: nitrogen-15 NMR study of gramicidin S in water and organic solvents, *J. Am. Chem. Soc. 106*, 1939−1941.
17. Bax, A., and Subramanian, S. (1986) Sensitivity-Enhanced Two-Dimensional Heteronuclear Shift Correlation NMR Spectroscopy, *J. Magn. Reson. 67*, 565−569.
18. Edison, A. S., Abildgaard, F., Westler, W. M., Mooberry, E. S., and Markley, J. L. (1994) Practical introduction to theory and implementation of multinuclear, multidimensional nuclear magnetic resonance experiment, *Methods Enzymol. 239*, 3−79.
19. Delaglio, F., Grzesiek, S., Vuister, G. W., Guang, Z., Pfeifer, J., and Bax, A. (1995) NMRPipe: A Multidimensional Spectral Processing System Based on UNIX Pipes, *J. Biomol. NMR 6*, 277−293.
20. Johnson, B. A., and Blevins, R. A. (1994) NMRView: A Computer Program for the Visualization and Analysis of NMR Data, *J. Biomol. NMR 4*, 603−614.
21. Garrett, D. S., Seok, Y.-J., Peterkofsky, A., Clore, G. M., and Gronenborn, A. M. (1997) Identification by NMR of the binding surface for the histidine-containing phosphocarrier protein HPr on the N-terminal domain of enzyme I of the *Escherichia coli* phosphotransferase system, *Biochemistry 36*, 4393−4398.
22. Bodenhausen, G., and Ruben, D. G. (1980) *Chem. Phys. Lett. 69*, 185−189.
23. Bax, A., Ikura, M., Kay, L. E., Torchia, D. A., and Tschudin, R. (1990) Comparison of Different Modes of Two-Dimensional Reverse-Correlation NMR for the Study of Proteins, *J. Magn. Reson. 86*, 304−318.
24. Vuister, G. W., and Bax, A. (1992) Resolution Enhancement and Spectral Editing of Uniformaly ^{13}C-Enriched Proteins by Homonulcear Broadband ^{13}C Decoupling, *J. Magn. Reson. 98*, 428−435.
25. Marion, D., Driscoll, P. C., Kay, L. E., Wingfield, P. T., Bax, A., Groenenborn, A. M., and Clore, G. M. (1989) Overcoming the overlap problem in the assignment of ^{1}H NMR spectra of larger proteins by use of three-dimensional heteronuclear ^{1}H-^{15}N Hartmann−Hahn-multiple quantum coherence and nuclear Overhauser-multiple quantum coherence spectroscopy: application to interleukin 1 beta, *Biochemistry 28*, 6150−6156.
26. Cavanagh, J., and Rance, M. (1992) Suppression of Cross-Relaxation Effects in TOCSY Spectra via a Modified DIPSI-2 Mixing Sequence, *J. Magn. Reson. 96*, 670−678.
27. Grzesiek, S., and Bax, A. (1992) An Efficient Experiment for Sequential Backbone Assignment of Medium-Sized Isotopically Enriched Proteins, *J. Magn. Reson. 99*, 201−207.
28. Grzesiek, S., and Bax, A. (1992) Correlating Backbone Amide and Side Chain Resonances in Larger Proteins by Multiple Relayed Triple Resonance NMR, *J. Am. Chem. Soc. 114*, 6291−6293.
29. Grzesiek, S., and Bax, A. (1993) Amino acid type determination in the sequential assignment procedure of uniformly ^{13}C/^{15}N-enriched proteins, *J. Biomol. NMR 3*, 185−204.
30. Knauf, M. A., Lohr, F., Curley, G. P., O'Farrell, P., Mayhew, S. G., Muller, F., and Ruterjans, H. (1993) Homonuclear and heteronuclear NMR studies of oxidized *Desulfovibrio vulgaris* flavodoxin. Sequential assignments and identification of secondary structure elements, *Eur. J. Biochem. 213*, 167−184.
31. Stockman, B. J., Euvrard, A., Kloosterman, D. A., Scahill, T. A., and Swenson, R. P. (1993) ^{1}H and ^{15}N resonance assignments and solution secondary structure of oxidized *Desulfovibrio vulgaris* flavodoxin determined by heteronuclear three-dimensional NMR spectroscopy, *J. Biomol. NMR 3*, 133−149.
32. Walsh, M. A., McCarthy, A., O'Farrell, P. A., McArdle, P., Cunningham, P. D., Mayhew, S. G., and Higgins, T. M. (1998) X-ray crystal structure of the *Desulfovibrio vulgaris* (Hildenborough) apoflavodoxin-riboflavin complex, *Eur. J. Biochem. 258*, 362−371.
33. Williams, T. C., Shelling, J. G., and Sykes, B. D. (1985) in *NMR in the Life Sciences* (Bradbury, E. M., and Nicolini, C., Eds.) pp 93−103, Plenum Press, New York.
34. Woody, R. W., and Dunker, A. K. (1996) in *Circular Dichroism and the Conformational Analysis of Biomolecules* (Fasman, G. D., Ed.) pp 136−144, Plenum Press, New York.
35. Koradi, R., Billeter, M., and Wuthrich, K. (1996) MOLMOL: a program for display and analysis of macromolecular structures, *J. Mol. Graphics 14*, 51−55.

BI026968K